Axial-flexural coupled vibration and buckling of composite beams using sinusoidal shear deformation theory

Thuc P. Vo[a,b,*], Huu-Tai Thai[c], Fawad Inam[a,b]

[a] *School of Mechanical, Aeronautical and Electrical Engineering, Glyndŵr University, Mold Road, Wrexham LL11 2AW, UK.*

[b] *Advanced Composite Training and Development Centre, Unit 5, Hawarden Industrial Park Deeside, Flintshire CH5 3US, UK.*

[c] *Department of Civil and Environmental Engineering, Hanyang University, 17 Haengdang-dong, Seongdong-gu, Seoul 133-791, Republic of Korea.*

Abstract

A finite element model based on sinusoidal shear deformation theory is developed to study vibration and buckling analysis of composite beams with arbitrary lay-ups. This theory satisfies the zero traction boundary conditions on the top and bottom surfaces of beam without using shear correction factors. Besides, it has strong similarity with Euler-Bernoulli beam theory in some aspects such as governing equations, boundary conditions, and stress resultant expressions. By using Hamilton's principle, governing equations of motion are derived. A displacement-based one-dimensional finite element model is developed to solve the problem. Numerical results for cross-ply and angle-ply composite beams are obtained as special cases and are compared with other solutions available in the literature. A variety of parametric studies are conducted to demonstrate the effect of fiber orientation and modulus ratio on the natural frequencies, critical buckling loads and corresponding mode shapes of composite beams.

Keywords: Composite beams; sinusoidal shear deformation theory; triply axial-flexural coupled; load-frequency curve.

1. Introduction

Composite materials are increasingly being used in various engineering applications due to their attractive properties in strength, stiffness, and lightness. The accurate prediction of stability and dynamic characteristics is of the fundamental importance in the design of composite structures. Finite element (FE) models originally developed for one-layered isotropic structures were extended to laminated composite structures as equivalent single-layer models. These models are known to provide a sufficiently accurate description of the global response of thin to moderately thick laminates [1]

*Corresponding author, tel.: +44 1978 293979

Email address: t.vo@glyndwr.ac.uk (Thuc P. Vo)

and considered in this paper. Thanks to the advantage that no shear correction factors are needed, the higher-order beam theory (HOBT) is widely used in the vibration analysis of composite beams. Soldatos and Elishakoff [2] developed this theory for static and dynamic analysis of composite beams. Chandrashekhara and Bangera [3] studied the free vibration characteristics of composite beams by using finite element. Marur et al. ([4]-[7]) studied vibration analysis of sandwich and composite beams using the HOBT through proper constitution of elasticity matrix. Shi and Lam [8] presented a FE formulation for the free vibration analysis of composite beams. Murthy et al. [9] developed a refined two-noded beam element with four degree-of-freedom per node for static and dynamic behaviour of asymmetric composite beams with different boundary conditions. Subramanian [10] formulated two theories using a two-noded C^1 continuous beam FE model with eight degree-of-freedom per node for dynamic analysis of symmetrical composite beams. Jun et al. ([11]-[13]) introduced the dynamic stiffness matrix method to solve the free vibration of axially loaded composite beams with arbitrary lay-ups. In the framework of a sinus models family, Vidal and Polit ([14], [15]) presented a three-noded multilayered (sandwich and laminated) beam element for static and dynamic analysis. Some researchers studied vibration and buckling problems in a unified fashion. Khdeir and Reddy ([16], [17]) utilised the state-space concept to solve the fundamental natural frequencies and critical buckling loads of composite beams for symmetric and anti-symmetric cross-ply lay-ups. Song and Waas [18] studied the buckling and free vibration of uniform and stepped unidirectionally laminated cantilever beams in which a cubic distribution of the displacement field through the beam thickness was assumed. Karama et.al ([19],[20]) presented bending, buckling and free vibration of composite beams with a transverse shear stress continuity model. By using the method of power series expansion of displacement components, Matsunaga [21] analyzed the natural frequencies and critical buckling loads of cross-ply composite beams. Aydogdu ([22]-[24]) carried out the vibration and buckling analysis of cross-ply and angle-ply composite beams in which a three degree-of-freedom shear deformable beam theory was developed based on Ritz method. Analytical solutions based on the global local higher-order theory for simply-supported boundary condition were derived by Zhen and Wanji [25] to study vibration and buckling of composite beams. Although there are many references available on free vibration and buckling analysis of composite beams, most of which deal with cross-ply, angle-ply composite beams. By using the sinusoidal shear deformation theory, the research on the natural frequencies, critical buckling loads and load-frequency curves as well as corresponding mode shapes of generally composite beams in a unitary manner is limited.

In this paper, which is extended from previous research [26], vibration and buckling analysis of composite beams using sinusoidal shear deformation theory is presented. This theory satisfies the

zero traction boundary conditions on the top and bottom surfaces of the beam without using shear correction factors. Besides, it has strong similarity with Euler-Bernoulli beam theory in some aspects such as governing equations, boundary conditions, and stress resultant expressions. By using Hamilton's principle, governing equations of motion are derived. A displacement-based one-dimensional finite element model is developed to solve the problem. Numerical results for cross-ply and angle-ply composite beams are obtained as special cases and are compared with other solutions available in the literature. A variety of parametric studies are conducted to demonstrate the effect of fiber orientation and modulus ratio on the natural frequencies, critical buckling loads and corresponding mode shapes of generally composite beams.

2. Kinematics

Consider a laminated composite beam with length L and rectangular cross section $b \times h$, with b being the width and h being the height. The x-, y-, and z-axes are taken along the length, width, and height of the beam, respectively. This composite beam is made of many plies of orthotropic materials in different orientations with respect to the x-axis. To derive the finite element model of composite beam, the following assumptions are made for the displacement field:

(a) The axial and transverse displacements consist of bending and shear components in which the bending components do not contribute toward shear forces and, likewise, the shear components do not contribute toward bending moments.

(b) The bending component of axial displacement is similar to that given by the Euler-Bernoulli beam theory.

(c) The shear component of axial displacement gives rise to the higher-order variation of shear strain and hence to shear stress through the depth of the beam in such a way that shear stress vanishes on the top and bottom surfaces.

The displacement field of the present study can be obtained by modifying the sinusoidal shear deformation theory based on Touratier [27] as:

$$U(x,z,t) = u(x,t) - z\frac{\partial w_b(x,t)}{\partial x} + \Big[z - \frac{h}{\pi}\sin(\frac{\pi z}{h})\Big]\frac{\partial w_s(x,t)}{\partial x} \tag{1a}$$

$$W(x,z,t) = w_b(x,t) + w_s(x,t) \tag{1b}$$

where u is the axial displacement along the mid-plane of the beam, w_b and w_s are the bending and shear components of transverse displacement along the mid-plane of the beam, respectively. The

non-zero strains are given by:

$$\epsilon_x = \frac{\partial U}{\partial x} = \epsilon_x^\circ + z\kappa_x^b + f\kappa_x^s \tag{2a}$$

$$\gamma_{xz} = \frac{\partial W}{\partial x} + \frac{\partial U}{\partial z} = (1 - f')\gamma_{xz}^\circ = g\gamma_{xz}^\circ \tag{2b}$$

where

$$f = z - \frac{h}{\pi}\sin(\frac{\pi z}{h}) \tag{3a}$$

$$g = 1 - f' = \cos(\frac{\pi z}{h}) \tag{3b}$$

and $\epsilon_x^\circ, \gamma_{xz}^\circ, \kappa_x^b$ and κ_x^s are the axial strain, shear strains and curvatures in the beam, respectively defined as:

$$\epsilon_x^\circ = u' \tag{4a}$$

$$\gamma_{xz}^\circ = w_s' \tag{4b}$$

$$\kappa_x^b = -w_b'' \tag{4c}$$

$$\kappa_x^s = -w_s'' \tag{4d}$$

where differentiation with respect to the x-axis is denoted by primes ($'$).

3. Variational Formulation

In order to derive the equations of motion, Hamilton's principle is used:

$$\delta \int_{t_1}^{t_2} (\mathcal{K} - \mathcal{U} - \mathcal{V}) dt = 0 \tag{5}$$

where $\mathcal{U}, \mathcal{V}$ and $\mathcal{K}$ denote the strain energy, potential energy, and kinetic energy, respectively.

The variation of the strain energy can be stated as:

$$\delta\mathcal{U} = \int_v (\sigma_x \delta\epsilon_x + \sigma_{xz}\delta\gamma_{xz}) dv = \int_0^l (N_x \delta\epsilon_z^\circ + M_x^b \delta\kappa_x^b + M_x^s \delta\kappa_x^s + Q_{xz}\delta\gamma_{xz}^\circ) dx \tag{6}$$

where N_x, M_x^b, M_x^s and Q_{xz} are the axial force, bending moments and shear force, respectively, defined by integrating over the cross-sectional area A as:

$$N_x = \int_A \sigma_x dA \tag{7a}$$

$$M_x^b = \int_A \sigma_x z dA \tag{7b}$$

$$M_x^s = \int_A \sigma_x f dA \tag{7c}$$

$$Q_{xz} = \int_A \sigma_{xz} g dA \tag{7d}$$

The variation of the potential energy of the axial force can be expressed as:

$$\delta\mathcal{V} = -\int_0^l P_0\Big[\delta w_b'(w_b'+w_s') + \delta w_s'(w_b'+w_s')\Big]dx \tag{8}$$

The variation of the kinetic energy is obtained as:

$$\begin{aligned}\delta\mathcal{K} &= \int_v \rho_k(\dot{U}\delta\dot{U} + \dot{W}\delta\dot{W})dv \\ &= \int_0^l \Big[\delta\dot{u}(m_0\dot{u} - m_1\dot{w_b}' - m_f\dot{w_s}') + \delta\dot{w_b}m_0(\dot{w_b}+\dot{w_s}) + \delta\dot{w_b}'(-m_1\dot{u} + m_2\dot{w_b}' + m_{fz}\dot{w_s}') \\ &+ \delta\dot{w_s}m_0(\dot{w_b}+\dot{w_s}) + \delta\dot{w_s}'(-m_f\dot{u} + m_{fz}\dot{w_b}' + m_{f^2}\dot{w_s}')\Big]dx \end{aligned} \tag{9}$$

where the differentiation with respect to the time t is denoted by dot-superscript convention and ρ_k is the density of a k^{th} layer and $m_0, m_1, m_2, m_f, m_{fz}$ and m_{f^2} are the inertia coefficients, defined by:

$$m_f = m_1 - \frac{h}{\pi}m_0^s \tag{10a}$$

$$m_{fz} = m_2 - \frac{h}{\pi}m_1^s \tag{10b}$$

$$m_{f^2} = m_2^s \tag{10c}$$

where

$$(m_0, m_1, m_2) = \int_A \rho_k(1, z, z^2)dA \tag{11a}$$

$$(m_0^s, m_1^s, m_2^s) = \int_A \rho_k\Big[\sin(\frac{\pi z}{h}), z\sin(\frac{\pi z}{h}), \cos^2(\frac{\pi z}{h})\Big]dA \tag{11b}$$

By substituting Eqs. (6), (8) and (9) into Eq. (5), the following weak statement is obtained:

$$\begin{aligned}0 &= \int_{t_1}^{t_2}\int_0^l \Big[\delta\dot{u}(m_0\dot{u} - m_1\dot{w_b}' - m_f\dot{w_s}') + \delta\dot{w_b}m_0(\dot{w_b}+\dot{w_s}) + \delta\dot{w_b}'(-m_1\dot{u} + m_2\dot{w_b}' + m_{fz}\dot{w_s}') \\ &+ \delta\dot{w_s}m_0(\dot{w_b}+\dot{w_s}) + \delta\dot{w_s}'(-m_f\dot{u} + m_{fz}\dot{w_b}' + m_{f^2}\dot{w_s}') \\ &+ P_0\big[\delta w_b'(w_b'+w_s') + \delta w_s'(w_b'+w_s')\big] - N_x\delta u' + M_x^b\delta w_b'' + M_x^s\delta w_s'' - Q_{xz}\delta w_s'\Big]dxdt \end{aligned} \tag{12}$$

4. Constitutive Equations

The stress-strain relations for the k^{th} lamina are given by:

$$\sigma_x = \bar{Q}_{11}\gamma_x \tag{13a}$$

$$\sigma_{xz} = \bar{Q}_{55}\gamma_{xz} \tag{13b}$$

where $\bar{Q}_{11}$ and $\bar{Q}_{55}$ are the elastic stiffnesses transformed to the x direction. More detailed explanation can be found in Ref. [28].

The constitutive equations for bar forces and bar strains are obtained by using Eqs. (2), (7) and (13):

$$\begin{Bmatrix} N_x \\ M_x^b \\ M_x^s \\ Q_{xz} \end{Bmatrix} = \begin{bmatrix} R_{11} & R_{12} & R_{13} & 0 \\ & R_{22} & R_{23} & 0 \\ & & R_{33} & 0 \\ \text{sym.} & & & R_{44} \end{bmatrix} \begin{Bmatrix} \epsilon_x^\circ \\ \kappa_x^b \\ \kappa_x^s \\ \gamma_{xz}^\circ \end{Bmatrix} \tag{14}$$

where R_{ij} are the laminate stiffnesses of general composite beams and given by:

$$R_{11} = \int_y A_{11} dy \tag{15a}$$

$$R_{12} = \int_y B_{11} dy \tag{15b}$$

$$R_{13} = \int_y (B_{11} - \frac{h}{\pi} E_{11}^s) dy \tag{15c}$$

$$R_{22} = \int_y D_{11} dy \tag{15d}$$

$$R_{23} = \int_y (D_{11} - \frac{h}{\pi} F_{11}^s) dy \tag{15e}$$

$$R_{33} = \int_y \big[D_{11} - 2\frac{h}{\pi} F_{11}^s + (\frac{h}{\pi})^2 G_{11}^s \big] dy \tag{15f}$$

$$R_{44} = \int_y H_{55}^s dy \tag{15g}$$

where A_{ij}, B_{ij} and D_{ij} matrices are the extensional, coupling and bending stiffness and $E_{ij}^s, F_{ij}^s, G_{ij}^s, H_{ij}^s$ matrices are the higher-order stiffnesses, respectively, defined by:

$$(A_{ij}, B_{ij}, D_{ij}) = \int_z \bar{Q}_{ij} (1, z, z^2) dz \tag{16a}$$

$$(E_{ij}^s, F_{ij}^s, G_{ij}^s, H_{ij}^s) = \int_z \bar{Q}_{ij} \Big[\sin(\frac{\pi z}{h}), z \sin(\frac{\pi z}{h}), \sin^2(\frac{\pi z}{h}), \cos^2(\frac{\pi z}{h}) \Big] dz \tag{16b}$$

$$H_{55}^s = \int_z \bar{Q}_{55} \cos^2(\frac{\pi z}{h}) dz \tag{16c}$$

5. Governing equations of motion

The equilibrium equations of the present study can be obtained by integrating the derivatives of the varied quantities by parts and collecting the coefficients of $\delta u, \delta w_b$ and δw_s:

$$N_x' = m_0 \ddot{u} - m_1 \ddot{w_b}' - m_f \ddot{w_s}' \tag{17a}$$

$$M_x^{b\prime\prime} - P_0(w_b'' + w_s'') = m_0(\ddot{w_b} + \ddot{w_s}) + m_1 \ddot{u}' - m_2 \ddot{w_b}'' - m_{fz} \ddot{w_s}'' \tag{17b}$$

$$M_x^{s\prime\prime} + Q_{xz}' - P_0(w_b'' + w_s'') = m_0(\ddot{w_b} + \ddot{w_s}) + m_f \ddot{u}' - m_{fz} \ddot{w_b}'' - m_{f^2} \ddot{w_s}'' \tag{17c}$$

The natural boundary conditions are of the form:

$$\delta u \;:\; N_x \tag{18a}$$

$$\delta w_b \;:\; M_x^{b\prime} - P_0(wb' + ws') - m_1\ddot{u} + m_2\ddot{w}_b{}' + m_{fz}\ddot{w}_s{}' \tag{18b}$$

$$\delta w_b' \;:\; M_x^b \tag{18c}$$

$$\delta w_s \;:\; M_x^{s\prime} + Q_{xz} - P_0(wb' + ws') - m_f\ddot{u} + m_{fz}\ddot{w}_b{}' + m_{f^2}\ddot{w}_s{}' \tag{18d}$$

$$\delta w_s' \;:\; M_x^s \tag{18e}$$

By substituting Eqs. (4) and (14) into Eq. (17), the explicit form of the governing equations of motion can be expressed with respect to the laminate stiffnesses R_{ij}:

$$R_{11}u'' - R_{12}w_b''' - R_{13}w_s''' = m_0\ddot{u} - m_1\ddot{w}_b{}' - m_f\ddot{w}_s{}' \tag{19a}$$

$$\begin{aligned} R_{12}u''' - R_{22}w_b^{iv} - R_{23}w_s^{iv} - P_0(w_b'' + w_s'') &= m_0(\ddot{w}_b + \ddot{w}_s) + m_1\ddot{u}' \\ &- m_2\ddot{w}_b{}'' - m_{fz}\ddot{w}_s{}'' \end{aligned} \tag{19b}$$

$$\begin{aligned} R_{13}u''' - R_{23}w_b^{iv} - R_{33}w_s^{iv} + R_{44}w_s'' - P_0(w_b'' + w_s'') &= m_0(\ddot{w}_b + \ddot{w}_s) + m_f\ddot{u}' \\ &- m_{fz}\ddot{w}_b{}'' - m_{f^2}\ddot{w}_s{}'' \end{aligned} \tag{19c}$$

Eq. (19) is the most general form for axial-flexural coupled vibration and buckling of composite beams, and the dependent variables, u, w_b and w_s are fully coupled. The resulting coupling is referred to as triply axial-flexural coupled vibration and buckling.

6. Finite Element Formulation

The present theory for composite beams described in the previous section was implemented via a displacement based finite element method. The variational statement in Eq. (12) requires that the bending and shear components of transverse displacement w_b and w_s be twice differentiable and C^1-continuous, whereas the axial displacement u must be only once differentiable and C^0-continuous. The generalized displacements are expressed over each element as a combination of the linear interpolation function Ψ_j for u and Hermite-cubic interpolation function ψ_j for w_b and w_s associated with node j and the nodal values:

$$u = \sum_{j=1}^{2} u_j\Psi_j \tag{20a}$$

$$w_b = \sum_{j=1}^{4} w_{bj}\psi_j \tag{20b}$$

$$w_s = \sum_{j=1}^{4} w_{sj}\psi_j \tag{20c}$$

Substituting these expressions in Eq. (20) into the corresponding weak statement in Eq. (12), the finite element model of a typical element can be expressed as the standard eigenvalue problem:

$$([K] - P_0[G] - \omega^2[M])\{\Delta\} = \{0\} \tag{21}$$

where $[K], [G]$ and $[M]$ are the element stiffness matrix, the element geometric stiffness matrix and the element mass matrix, respectively. The explicit forms of $[K]$ can be found in Ref. [26] and of $[G]$ and $[M]$ are given by:

$$G_{ij}^{22} = \int_0^l \psi_i'\psi_j' dz \tag{22a}$$

$$G_{ij}^{23} = \int_0^l \psi_i'\psi_j' dz \tag{22b}$$

$$G_{ij}^{33} = \int_0^l \psi_i'\psi_j' dz \tag{22c}$$

$$M_{ij}^{11} = \int_0^l m_0\Psi_i\Psi_j dz \tag{22d}$$

$$M_{ij}^{12} = -\int_0^l m_1\Psi_i\psi_j' dz \tag{22e}$$

$$M_{ij}^{13} = -\int_0^l m_f\Psi_i\psi_j' dz \tag{22f}$$

$$M_{ij}^{22} = \int_0^l (m_0\psi_i\psi_j + m_2\psi_i'\psi_j') dz \tag{22g}$$

$$M_{ij}^{23} = \int_0^l (m_0\psi_i\psi_j + m_{fz}\psi_i'\psi_j') dz \tag{22h}$$

$$M_{ij}^{33} = \int_0^l (m_0\psi_i\psi_j + m_{f^2}\psi_i'\psi_j') dz \tag{22i}$$

All other components are zero. In Eq.(21), $\{\Delta\}$ is the eigenvector of nodal displacements corresponding to an eigenvalue:

$$\{\Delta\} = \{u\ w_b\ w_s\}^{\mathrm{T}} \tag{23}$$

7. Numerical Examples

For verification purpose, vibration analysis of symmetric cross-ply $[0°/90°/90°/0°]$ and anti-symmetric angle-ply $[45°/-45°/45°/-45°]$ composite beams with various boundary conditions is performed. The material properties are assumed to be: $E_1 = 144.9\text{GPa}, E_2 = 9.65\text{GPa}, G_{12} = G_{13} = 4.14\text{GPa}, G_{23} =$

3.45GPa, $\nu_{12} = 0.3$, $\rho = 1389\text{kg/m}^3$. The boundary conditions of beam are presented by C for clamped edge: $u = w_b = w_b' = w_s = w_s' = 0$, S for simply-supported edge: $u = w_b = w_s = 0$ and F for free edge. The first three non-dimensional natural frequencies are tabulated in Table 1 and the non-dimensional term is defined by: $\overline{\omega} = \dfrac{\omega L^2}{h}\sqrt{\dfrac{\rho}{E_1}}$. An excellent agreement between the predictions of the present model and the results of the other models mentioned ([3], [7], [8], [29]) can be observed.

To demonstrate the accuracy and validity of this study further, symmetric cross-ply [0°/90°/0°] and anti-symmetric cross-ply [0°/90°] composite beams with cantilever and simply-supported boundary conditions are considered. In the following examples, all laminate are of equal thickness and made of the same orthotropic material, whose properties are:

$$E_1/E_2 = \text{open}, G_{12} = G_{13} = 0.6E_2, G_{23} = 0.5E_2, \nu_{12} = 0.25 \tag{24}$$

For convenience, the following non-dimensional terms are used in presenting the numerical results:

$$\overline{P}_{cr} = \frac{P_{cr}L^2}{E_2 b h^3} \tag{25a}$$

$$\overline{\omega} = \frac{\omega L^2}{h}\sqrt{\frac{\rho}{E_2}} \tag{25b}$$

The fundamental natural frequencies and critical buckling loads for different span-to-height (L/h) ratios are compared with analytical solutions ([16], [17]) and previous results ([9], [22], [23]) in Tables 2 and 3. Material with $E_1/E_2 = 10$ and 40 is used. Through the close correlation observed between the present model and the earlier works, accuracy and adequacy of the present model is again established. The critical buckling loads increase as modulus ratio increases (Table 3). Effect of L/h ratio on the critical buckling loads and fundamental natural frequencies is plotted in Figs. 1 and 2. It is clear that shear effects on a symmetric cross-ply lay-up are more pronounced than an anti-symmetric one for a given L/h ratio. For a symmetric cross-ply lay-up with simply-supported boundary condition, the present theory becomes effective in a relatively large region up to the point where span-to-height ratio reaches value of $L/h = 40$. Thus, a span-to-height ratio $L/h = 10$ is chosen to show effect of the axial force on the fundamental natural frequencies. Load-frequency curves of symmetric and anti-symmetric cross-ply composite beams with $E_1/E_2 = 10$ and 40 are illustrated in Fig. 3. As expected, the natural frequency diminishes when the axial force increases. It is obvious that the load-frequency curves decrease rapidly prior to the critical buckling loads and finally, the natural frequencies vanish at these loads. Four load-frequency curves are observed (Fig. 3). The smallest curve is for an anti-symmetric cross-ply cantilever beam and the largest one is for a symmetric cross-ply simply-supported beam. Besides, Fig. 3 also explains the duality between the buckling load and natural frequency.

In order to investigate the effects of fiber orientation on the natural frequencies, critical buckling

loads and load-frequency curves as well as corresponding mode shapes, a clamped-clamped anti-symmetric angle-ply $[\theta/-\theta]$ composite beam is considered. Unless mentioned otherwise, $L/h = 10$ and material with $E_1/E_2 = 40$ is used for the analysis. The first four natural frequencies and critical buckling loads with respect to the fiber angle change are shown in Table 4. The uncoupled solution, which neglects the coupling effects coming from the material anisotropy, are also given. The natural frequencies and buckling loads decrease monotonically with the increase of the fiber angle. As the fiber angle increases, the buckling loads decrease more quickly than natural frequencies. The uncoupled solution might not be accurate. However, since coupling effects are negligible for this lay-up, the results by uncoupled and coupled solution are identical (Table 4), which implies that the uncoupled solution is sufficiently accurate for this lay-up. The first, second, third and fourth flexural vibration mode shapes with the fiber angle $\theta = 30^\circ$ are illustrated in Fig. 4. The first flexural buckling mode with various fiber angles $\theta = 0^\circ, 30^\circ$ and 60° are also given in Fig. 5. It is clear that all the mode shapes exhibit double coupling (bending and shear components of transverse displacement). The load-frequency curves of these fiber angles is exhibited in Fig. 6. Characteristic of load-frequency curves is that the value of the axial force for which the natural frequency vanishes constitutes the buckling load. Thus, when the fiber angle is equal to 0°, 30° and 60°, the first flexural buckling occurs at about P = 37.274, 16.980 and 3.735, respectively.

The next example is the same as before except that in this case, an unsymmetric $[0^\circ/\theta]$ lay-up is considered. For this lay-up, the coupling stiffnesses $R_{12}, R_{13}, R_{14}, R_{23}$ and R_{24} do not vanish. A comprehensive three dimensional interaction diagram of the fundamental natural frequency, axial force and fiber angle of two lay-ups $[\theta/-\theta]$ and $[0^\circ/\theta]$ is plotted in Fig. 7. It is clear that the presence of the 0° layer in the $[0^\circ/\theta]$ configuration increases the natural frequency and buckling load as well as load-frequency curve with increasing fiber angle. As seen in Table 5 and Fig. 8, the uncoupled and coupled solution shows discrepancy indicating the coupling effects become significant as the fiber angle increases. It can be remarked again in Fig. 8 that the natural frequencies decrease with the increase of axial forces, and the decrease becomes more quickly when axial forces are close to buckling loads. The vibration and buckling mode shapes are illustrated in Figs. 9 and 10. Due to strong coupling effects, triply coupled mode (axial, bending and shear components) can be observed. This fact explains that the uncoupled solution is no longer valid for unsymmetric composite beams, and triply axial-flexural coupled vibration and buckling should be considered simultaneously for accurate analysis of composite beams.

Finally, the effects of modulus ratio (E_1/E_2) on the first three natural frequencies of a cantilever composite beam under an axial compressive force and tensile force $(P = \pm 0.5 P_{cr})$ are investigated. A

symmetric cross-ply [0°/90°/0°] and an anti-symmetric cross-ply [0°/90°] lay-ups are considered. It is observed from Fig. 11 that the natural frequencies increase with increasing orthotropy (E_1/E_2) for two lay-ups considered.

8. Conclusions

A theoretical model based sinusoidal shear deformation theory is presented to study vibration and buckling of composite beams with arbitrary lay-ups. This model is capable of predicting accurately the natural frequencies, critical buckling loads and corresponding mode shapes for various configurations. It accounts for the parabolical variation of shear strains through the depth of the beam, and satisfies the zero traction boundary conditions on the top and bottom surfaces of the beam without using shear correction factor. To formulate the problem, a two-noded C^1 beam element with five degree-of-freedom per node which accounts for shear effects and all coupling effects coming from the material anisotropy is developed. All of the possible vibration and buckling modes including the axial and flexural mode as well as triply axial-flexural coupled mode are included in the analysis. The present model is found to be appropriate and efficient in analyzing vibration and buckling problem of composite beams.

9. References

References

[1] J. N. Reddy, Mechanics of laminated composite plates and shells: theory and analysis, CRC, 2004.

[2] K. Soldatos, I. Elishakoff, A transverse shear and normal deformable orthotropic beam theory, Journal of Sound and Vibration 155 (3) (1992) 528 – 533.

[3] K. Chandrashekhara, K. Bangera, Free vibration of composite beams using a refined shear flexible beam element, Computers and Structures 43 (4) (1992) 719 – 727.

[4] S. R. Marur, T. Kant, Free vibration analysis of fiber reinforced composite beams using higher order theories and finite element modelling, Journal of Sound and Vibration 194 (3) (1996) 337 – 351.

[5] T. Kant, S. R. Marur, G. S. Rao, Analytical solution to the dynamic analysis of laminated beams using higher order refined theory, Composite Structures 40 (1) (1997) 1 – 9.

[6] S. R. Marur, T. Kant, A higher order finite element model for the vibration analysis of laminated beams, Journal of Vibration and Acoustics 120 (3) (1998) 822–824.

[7] S. R. Marur, T. Kant, On the angle ply higher order beam vibrations, Computational Mechanics 40 (2007) 25–33.

[8] G. Shi, K. Y. Lam, Finite element vibration analysis of composite beams based on higher-order beam theory, Journal of Sound and Vibration 219 (4) (1999) 707 – 721.

[9] M. V. V. S. Murthy, D. R. Mahapatra, K. Badarinarayana, S. Gopalakrishnan, A refined higher order finite element for asymmetric composite beams, Composite Structures 67 (1) (2005) 27 – 35.

[10] P. Subramanian, Dynamic analysis of laminated composite beams using higher order theories and finite elements, Composite Structures 73 (3) (2006) 342 – 353.

[11] L. Jun, L. Xiaobin, H. Hongxing, Free vibration analysis of third-order shear deformable composite beams using dynamic stiffness method, Archive of Applied Mechanics 79 (2009) 1083–1098.

[12] L. Jun, H. Hongxing, Dynamic stiffness analysis of laminated composite beams using trigonometric shear deformation theory, Composite Structures 89 (3) (2009) 433 – 442.

[13] L. Jun, H. Hongxing, Free vibration analyses of axially loaded laminated composite beams based on higher-order shear deformation theory, Meccanica 46 (2011) 1299–1317.

[14] P. Vidal, O. Polit, A family of sinus finite elements for the analysis of rectangular laminated beams, Composite Structures 84 (1) (2008) 56 – 72.

[15] P. Vidal, O. Polit, Vibration of multilayered beams using sinus finite elements with transverse normal stress, Composite Structures 92 (6) (2010) 1524 – 1534.

[16] A. A. Khdeir, J. N. Reddy, Free vibration of cross-ply laminated beams with arbitrary boundary conditions, International Journal of Engineering Science 32 (12) (1994) 1971–1980.

[17] A. A. Khdeir, J. N. Reddy, Buckling of cross-ply laminated beams with arbitrary boundary conditions, Composite Structures 37 (1) (1997) 1 – 3.

[18] S. J. Song, A. M. Waas, Effects of shear deformation on buckling and free vibration of laminated composite beams, Composite Structures 37 (1) (1997) 33 – 43.

[19] M. Karama, B. A. Harb, S. Mistou, S. Caperaa, Bending, buckling and free vibration of laminated composite with a transverse shear stress continuity model, Composites Part B: Engineering 29 (3) (1998) 223 – 234.

[20] M. Karama, K. S. Afaq, S. Mistou, Mechanical behaviour of laminated composite beam by the new multi-layered laminated composite structures model with transverse shear stress continuity, International Journal of Solids and Structures 40 (6) (2003) 1525 – 1546.

[21] H. Matsunaga, Vibration and buckling of multilayered composite beams according to higher order deformation theories, Journal of Sound and Vibration 246 (1) (2001) 47 – 62.

[22] M. Aydogdu, Vibration analysis of cross-ply laminated beams with general boundary conditions by Ritz method, International Journal of Mechanical Sciences 47 (11) (2005) 1740 – 1755.

[23] M. Aydogdu, Buckling analysis of cross-ply laminated beams with general boundary conditions by Ritz method, Composites Science and Technology 66 (10) (2006) 1248 – 1255.

[24] M. Aydogdu, Free vibration analysis of angle-ply laminated beams with general boundary conditions, Journal of Reinforced Plastics and Composites 25 (15) (2006) 1571–1583.

[25] W. Zhen, C. Wanji, An assessment of several displacement-based theories for the vibration and stability analysis of laminated composite and sandwich beams, Composite Structures 84 (4) (2008) 337 – 349.

[26] T. P. Vo and H. T. Thai, Static behaviour of composite beams using various refined shear deformation theories. Composite Structures 94 (8) (2012) 2513–2522

[27] M. Touratier, An efficient standard plate theory, International Journal of Engineering Science 29 (8) (1991) 901 – 916.

[28] R. M. Jones, Mechanics of Composite Materials, Taylor & Francis, 1999.

[29] W. Q. Chen, C. F. Lv, Z. G. Bian, Free vibration analysis of generally laminated beams via state-space-based differential quadrature, Composite Structures 63 (3-4) (2004) 417 – 425.

Figure 1: Effect of span-to-height ratio on the non-dimensional fundamental natural frequencies of a symmetric and anti-symmetric cross-ply composite beam with cantilever and simply-supported boundary conditions ($E_1/E_2 = 40$).

Figure 2: Effect of span-to-height ratio on the non-dimensional critical buckling loads of a symmetric and anti-symmetric cross-ply composite beam with cantilever and simply-supported boundary conditions ($E_1/E_2 = 40$).

Figure 3: Load-frequency curves of symmetric and anti-symmetric cross-ply composite beams with $E_1/E_2 = 10$ and 40 ($L/h = 10$).

Figure 4: Vibration mode shapes of the axial and flexural components of a clamped-clamped anti-symmetric angle-ply composite beam with the fiber angle 30°.

Figure 5: Buckling mode shapes of the axial and flexural components of a clamped-clamped anti-symmetric angle-ply composite beam with the fiber angles 0°, 30° and 60°.

Figure 6: Load-frequency curves of a clamped-clamped anti-symmetric angle-ply composite beam with the fiber angles 0°, 0° and 60°.

Figure 7: Three dimensional interaction diagram between the axial force and fundamental natural frequency of clamped composite beams with respect to the fiber angle change.

Figure 8: Load-frequency interaction curves of a clamped-clamped un-symmetric composite beam with the fiber angles 30° and 60°.

Figure 9: Vibration mode shapes of the axial and flexural components of a clamped-clamped un-symmetric composite beam with the fiber angle 60°.

Figure 10: Buckling mode shapes of the axial and flexural components of a clamped-clamped un-symmetric composite beam with the fiber angles 30° and 60°.

Figure 11: Variation of the first three natural frequencies with respect to modulus ratio change of a cantilever composite beam under an axial compressive force $P = 0.5P_{cr}$ and tensile force $P = -0.5P_{cr}$.

Table 1: The first five non-dimensional natural frequencies and buckling loads of composite beams with different boundary conditions.

Table 2: Effect of span-to-height ratios on the non-dimensional fundamental frequencies of a symmetric and anti-symmetric cross-ply composite beam with cantilever and simply-supported boundary conditions ($E_1/_E 2 = 40$).

Table 3: Effect of span-to-height ratios on the non-dimensional critical buckling loads of a symmetric and an anti-symmetric cross-ply composite beam with cantilever and simply-supported boundary conditions ($E_1/E_2 = 10$ and 40).

Table 4: The first four non-dimensional natural frequencies and critical buckling loads of a clamped-clamped anti-symmetric angle-ply $[\theta/-\theta]$ composite beam with respect to the fiber angle change.

Table 5: The first four non-dimensional natural frequencies and critical buckling loads of an unsymmetric $[0°/\theta]$ clamped-clamped composite beam with respect to the fiber angle change.

CAPTIONS OF TABLES

Table 1: The first three non-dimensional fundamental natural frequencies of composite beams with different boundary conditions (L/h=15).

Table 2: Effect of span-to-height ratio on the non-dimensional fundamental natural frequencies of a symmetric and anti-symmetric cross-ply composite beam with cantilever and simply-supported boundary conditions ($E_1/E_2 = 40$).

Table 3: Effect of span-to-height ratio on the non-dimensional critical buckling loads of a symmetric and an anti-symmetric cross-ply composite beam with cantilever and simply-supported boundary conditions ($E_1/E_2 = 10$ and 40).

Table 4: The first four non-dimensional natural frequencies and critical buckling loads of a clamped-clamped anti-symmetric angle-ply $[\theta/-\theta]$ composite beam with respect to the fiber angle change.

Table 5: The first four non-dimensional naturalfrequencies and critical buckling loads of an unsymmetric $[0/\theta]$ clamped-clamped composite beam with respect to the fiber angle change.

Table 1: The first three non-dimensional fundamental natural frequencies of composite beams with different boundary conditions (L/h=15).

Lay-ups	Boundary conditions	Reference	ω_1	ω_2	ω_3
$[0^0/90^0/90^0/0^0]$	CC	Shi and Lam [8]	4.6194	10.4162	17.1724
		Present	4.6342	10.9232	17.5753
	SS	Shi and Lam [8]	2.4979	8.4364	15.5932
		Present	2.4960	8.4815	15.8681
	CF	Marur and Kant [7]	0.9214	4.8919	11.4758
		Shi and Lam [8]	0.9199	4.9054	11.4886
		Present	0.9222	4.9165	11.5999
	CS	Shi and Lam [8]	3.5264	9.4736	16.4201
		Present	3.6049	9.6424	16.8138
$[45^0/-45^0/45^0/-45^0]$	CC	Chandrashekhara and Bangera [3]	1.9807	5.2165	9.6912
		Chen et al. [29]	1.8446	4.9871	9.5395
		Present	1.9921	5.2870	9.6852
	SS	Chandrashekhara and Bangera [3]	0.8278	3.2334	7.0148
		Chen et al. [29]	0.7998	3.1638	6.9939
		Present	0.9078	3.5257	7.5877
	CF	Chandrashekhara and Bangera [3]	0.2962	1.8156	4.9163
		Chen et al. [29]	0.2969	1.7778	4.8953
		Present	0.3253	1.9823	5.3270
	CS	Chandrashekhara and Bangera [3]	1.2786	4.0139	8.0261
		Present	1.4020	4.3667	8.6507

Table 2: Effect of span-to-height ratio on the non-dimensional fundamental natural frequencies of a symmetric and anti-symmetric cross-ply composite beam with cantilever and simply-supported boundary conditions ($E_1/E_2 = 40$).

Lay-ups	Boundary conditions	Reference	L/h		
			5	10	20
$[0^0/90^0/0^0]$	CF	Murthy et al. [9]	4.230	5.491	-
		Khdeir and Reddy [16]	4.234	5.495	-
		Aydogdu [22]	4.233	-	6.070
		Present	4.248	5.493	6.063
	SS	Murthy et al. [9]	9.207	13.614	-
		Khdeir and Reddy [16]	9.208	13.614	-
		Aydogdu [22]	9.207	-	16.337
		Present	9.294	13.616	16.326
$[0^0/90^0]$	CF	Murthy et al. [9]	2.378	2.541	-
		Khdeir and Reddy [16]	2.386	2.544	-
		Aydogdu [22]	2.384	-	2.590
		Present	2.387	2.543	2.589
	SS	Murthy et al. [9]	6.045	6.908	-
		Khdeir and Reddy [16]	6.128	6.945	-
		Aydogdu [22]	6.144	-	7.218
		Present	6.090	6.918	7.207

Table 3: Effect of span-to-height ratio on the non-dimensional critical buckling loads of a symmetric and an anti-symmetric cross-ply composite beam with cantilever and simply-supported boundary conditions (E_1/E_2 = 10 and 40).

Lay-ups and E_1/E_2 ratio	Boundary conditions	Reference	L/h		
			5	10	20
E_1/E_2 = 10					
$[0^0/90^0/0^0]$	CF	Aydogdu [23]	1.704	-	1.979
		Present	1.694	1.905	1.966
	SS	Aydogdu [23]	4.726	-	7.666
		Present	4.710	6.777	7.620
$[0^0/90^0]$	CF	Aydogdu [23]	0.542	-	0.565
		Present	0.539	0.557	0.562
	SS	Aydogdu [23]	1.919	-	2.241
		Present	1.914	2.157	2.228
E_1/E_2 = 40					
$[0^0/90^0/0^0]$	CF	Khdeir and Reddy [17]	4.708	6.772	-
		Aydogdu [23]	4.708	-	7.611
		Present	4.704	6.762	7.599
	SS	Khdeir and Reddy [17]	8.613	18.832	-
		Aydogdu [23]	8.613	-	27.084
		Present	8.640	18.817	27.047
$[0^0/90^0]$	CF	Aydogdu [23]	1.236	-	1.349
		Present	1.237	1.323	1.347
	SS	Aydogdu [23]	3.906	-	5.296
		Present	3.935	4.948	5.294

Table 4: The first four non-dimensional natural frequencies and critical buckling loads of a clamped-clamped anti-symmetric angle-ply $[\theta/-\theta]$ composite beam with respect to the fiber angle change.

Fiber angle	No coupling					With coupling				
	ω_{z_1}	ω_{z_2}	ω_{z_3}	ω_{z_4}	P_{z_1}	ω_1	ω_2	ω_3	ω_4	P_{cr}
0^0	20.650	45.002	71.529	103.875	37.274	20.650	45.002	71.529	103.875	37.274
15^0	19.548	43.065	68.319	99.104	33.375	19.548	43.065	68.319	99.104	33.375
30^0	14.153	33.654	54.824	80.924	16.980	14.153	33.654	54.824	80.924	16.980
45^0	8.856	22.667	39.537	47.334	6.423	8.856	22.667	39.537	47.334	6.423
60^0	6.788	17.766	31.945	35.007	3.735	6.788	17.766	31.945	35.007	3.735
75^0	6.241	16.409	29.710	31.966	3.151	6.241	16.409	29.710	31.966	3.151
90^0	6.141	16.155	29.278	31.424	3.050	6.141	16.155	29.278	31.424	3.050

Table 5: The first four non-dimensional naturalfrequencies and critical buckling loads of an unsymmetric $[0/\theta]$ clamped-clamped composite beam with respect to the fiber angle change.

Fiber angle	No coupling					With coupling				
	ω_{z_1}	ω_{z_2}	ω_{z_3}	ω_{z_4}	P_{z_1}	ω_1	ω_2	ω_3	ω_4	P_{cr}
0^0	20.650	45.002	71.529	103.875	37.274	20.650	45.002	71.529	103.875	37.274
15^0	20.147	44.107	70.021	101.602	35.479	20.108	44.063	69.971	101.564	35.324
30^0	18.760	41.698	66.168	96.038	30.672	17.490	40.014	64.288	94.332	26.264
45^0	18.175	40.616	64.493	93.671	28.746	14.920	35.808	59.163	88.376	18.713
60^0	17.967	40.156	63.764	92.614	28.089	14.019	34.155	57.099	85.851	16.417
75^0	17.862	39.897	63.347	92.000	27.766	13.786	33.683	56.448	84.989	15.857
90^0	17.827	39.807	63.202	91.786	27.659	13.739	33.578	56.290	84.767	15.747

CAPTIONS OF FIGURES

Figure 1: Effect of span-to-height ratio on the non-dimensional fundamental natural frequencies of symmetric cross-ply $[0^0/90^0/0^0]$ and anti-symmetric cross-ply $[0^0/90^0]$ composite beams with cantilever and simply-supported boundary conditions ($E_1/E_2 = 40$).

Figure 2: Effect of span-to-height ratio on the non-dimensional critical buckling loads of symmetric cross-ply $[0^0/90^0/0^0]$ and anti-symmetric cross-ply $[0^0/90^0]$ composite beams with cantilever and simply-supported boundary conditions ($E_1/E_2 = 40$).

Figure 3: Load-frequency curves of symmetric cross-ply $[0^0/90^0/0^0]$ and anti-symmetric cross-ply $[0^0/90^0]$ composite beams with $E_1/E_2 = 10$ and 40 (L/h = 10).

Figure 4: Vibration mode shapes of the axial and flexural components of a clamped-clamped anti-symmetric angle-ply $[\theta/-\theta]$ composite beam with the fiber angle 30^0.

Figure 5: Buckling mode shapes of the axial and flexural components of a clamped-clamped anti-symmetric angle-ply $[\theta/-\theta]$ composite beam with the fiber angles 0, 30^0 and 60^0.

Figure 6: Load-frequency curves of a clamped-clamped anti-symmetric angle-ply $[\theta/-\theta]$ composite beam with the fiber angles 0, 30^0 and 60^0.

Figure 7: Three dimensional interaction diagram of the fundamental natural frequency, axial force and fiber angle of clamped-clamped composite beams with $[\theta/-\theta]$ and $[0/\theta]$ lay-ups.

Figure 8: Load-frequency curves of a clamped-clamped unsymmetric $[0/\theta]$ composite beam with the fiber angles 30^0 and 60^0.

Figure 9: Vibration mode shapes of the axial and flexural components of a clamped-clamped un-symmetric $[0/\theta]$ composite beam with the fiber angle 60^0.

Figure 10: Buckling mode shapes of the axial and flexural components of a clamped-clamped un-symmetric $[0/\theta]$ composite beam with the fiber angles 30^0 and 60^0.

Figure 11: Variation of the first three natural frequencies with respect to modulus ratio change of a cantilever composite beam under an axial compressive force $P=0.5P_{cr}$ and tensile force $P=-0.5P_{cr}$

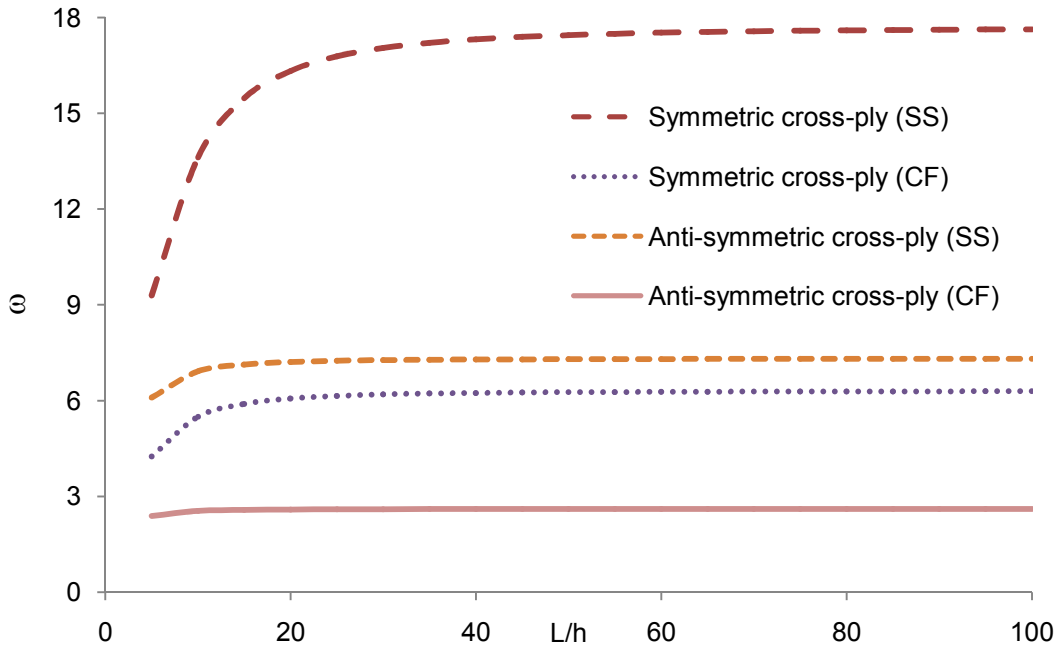

Figure 1: Effect of span-to-height ratio on the non-dimensional fundamental natural frequencies of symmetric cross-ply $[0^0/90^0/0^0]$ and anti-symmetric cross-ply $[0^0/90^0]$ composite beams with cantilever and simply-supported boundary conditions ($E_1/E_2 = 40$).

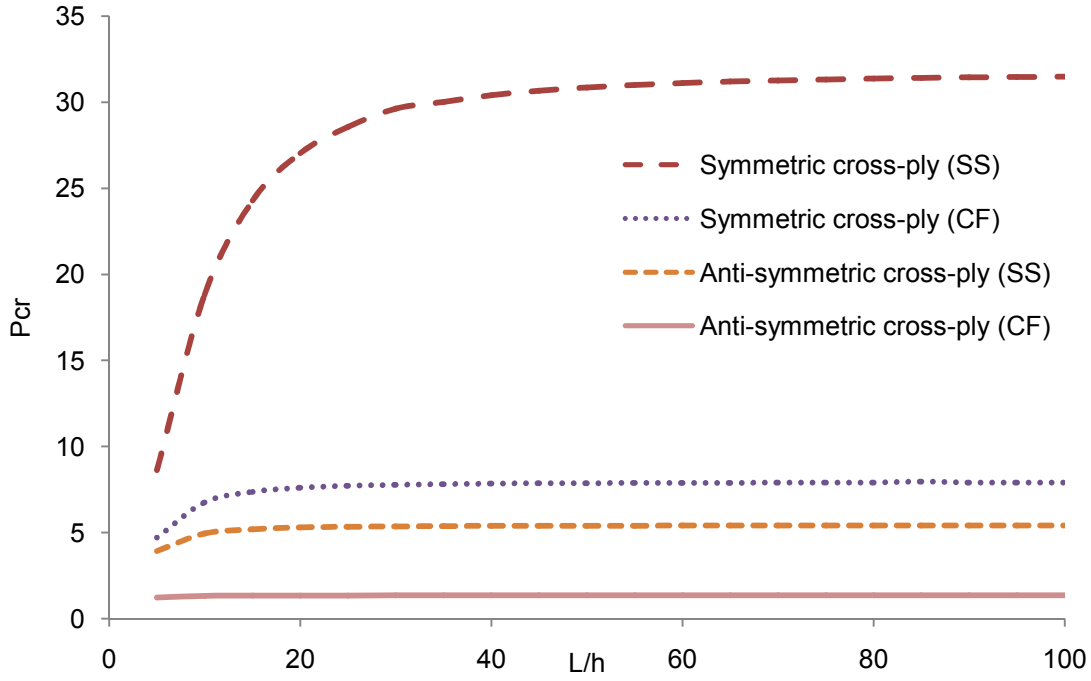

Figure 2: Effect of span-to-height ratio on the non-dimensional critical buckling loads of symmetric cross-ply $[0^0/90^0/0^0]$ and anti-symmetric cross-ply $[0^0/90^0]$ composite beams with cantilever and simply-supported boundary conditions ($E_1/E_2 = 40$).

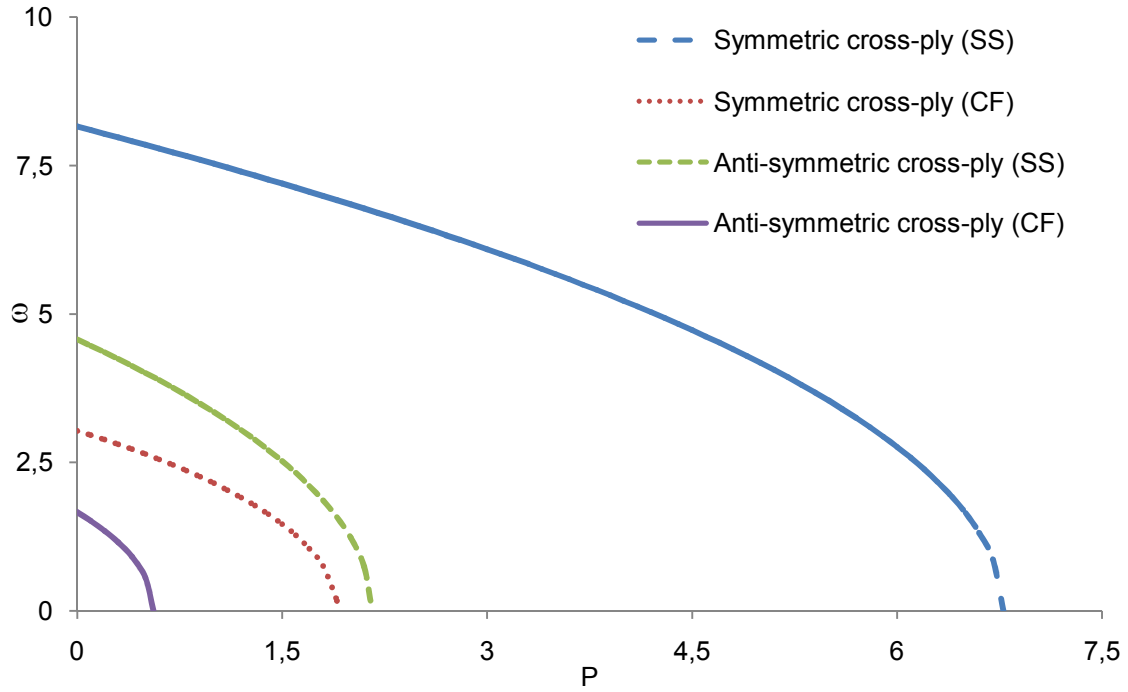

a. $E_1/E_2 = 10$

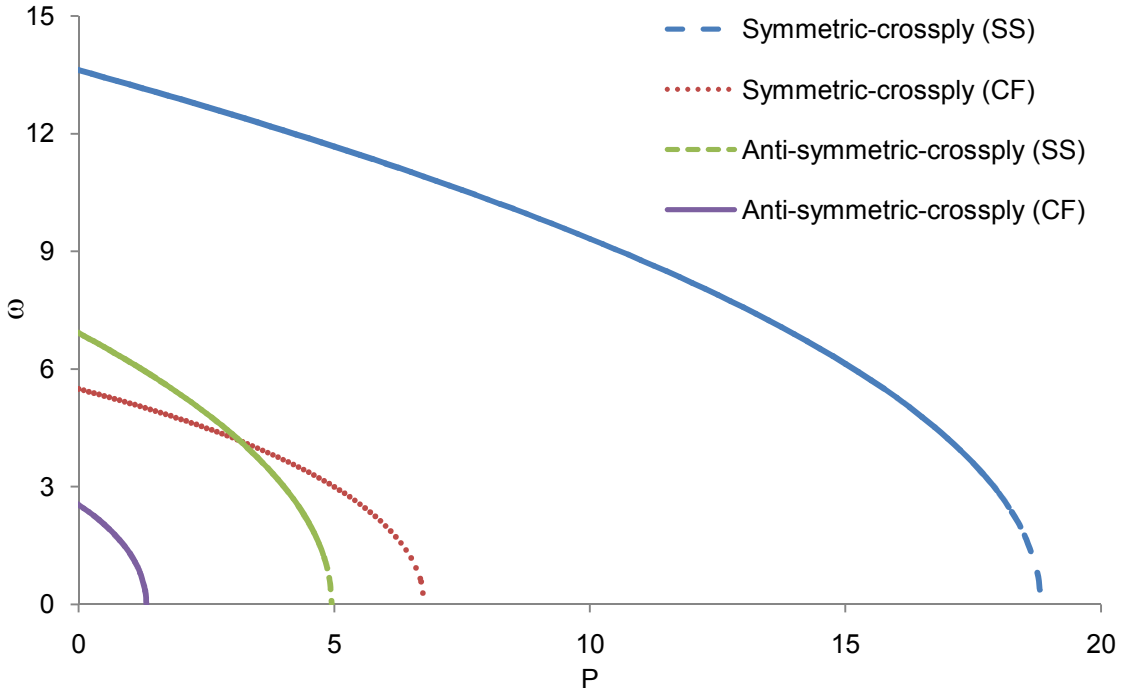

b. $E_1/E_2 = 40$

Figure 3: Load-frequency curves of symmetric cross-ply $[0^0/90^0/0^0]$ and anti-symmetric cross-ply $[0^0/90^0]$ composite beams with $E_1/E_2 = 10$ and 40 (L/h = 10).

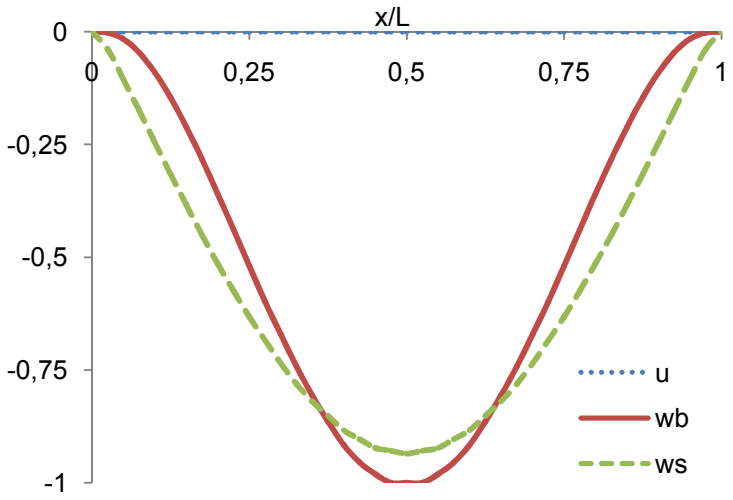

a. First mode shape $\omega_1 = 14.153$.

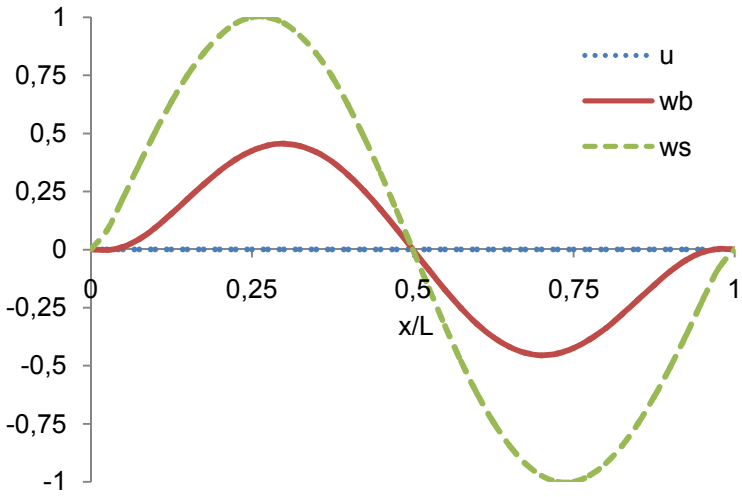

b. Second mode shape $\omega_2 = 33.654$.

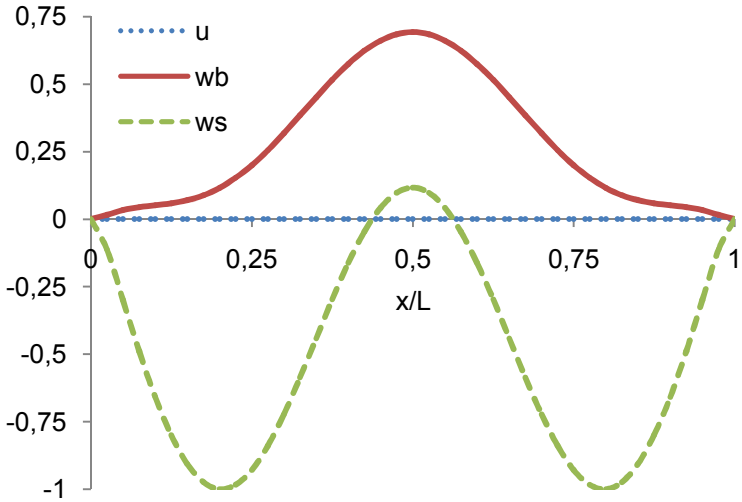

c. Third mode shape $\omega_3 = 54.824$.

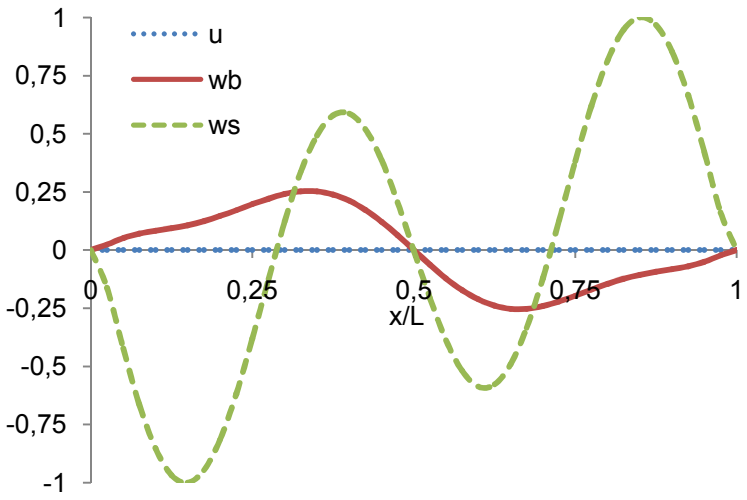

d. Fourth mode shape $\omega_4 = 80.924$

Figure 4: Vibration mode shapes of the axial and flexural components of a clamped-clamped anti-symmetric angle-ply $[\theta/-\theta]$ composite beam with the fiber angle 30^0.

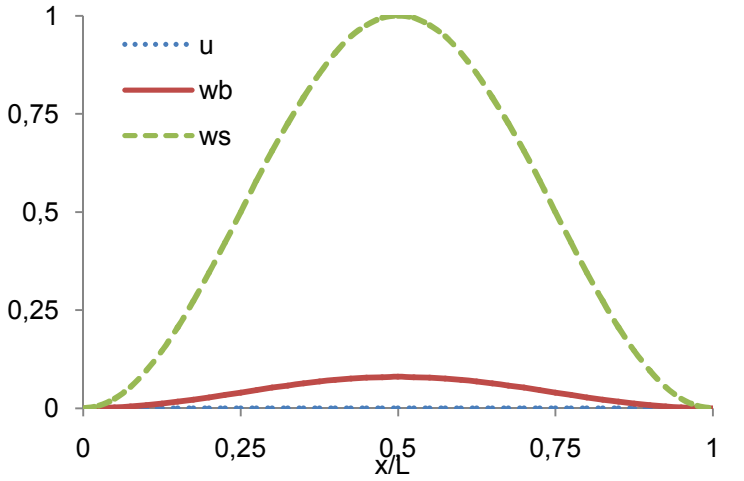

a. P_{cr} = 37.274 with the fiber angle 0^0.

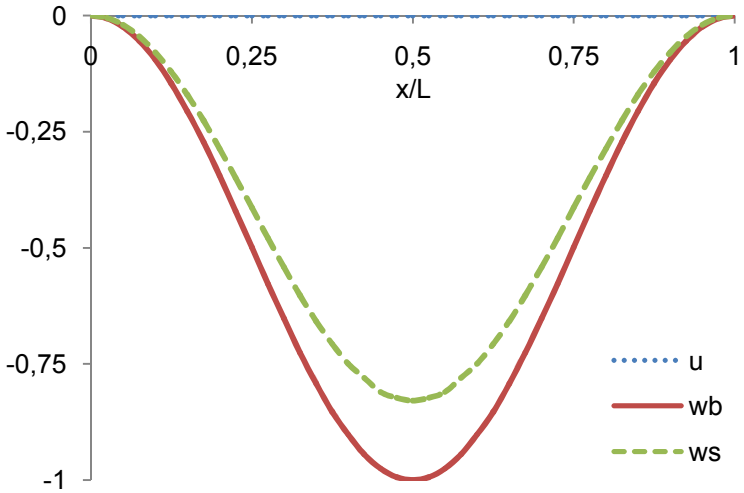

b. P_{cr} = 16.980 with the fiber angle 30^0.

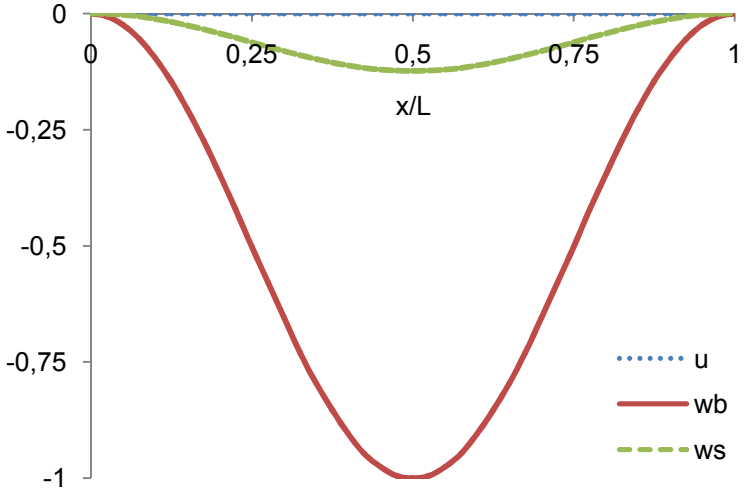

c. P_{cr} = 3.735 with the fiber angle 60^0.

Figure 5: Buckling mode shapes of the axial and flexural components of a clamped-clamped anti-symmetric angle-ply $[\theta/-\theta]$ composite beam with the fiber angles 0, 30^0 and 60^0.

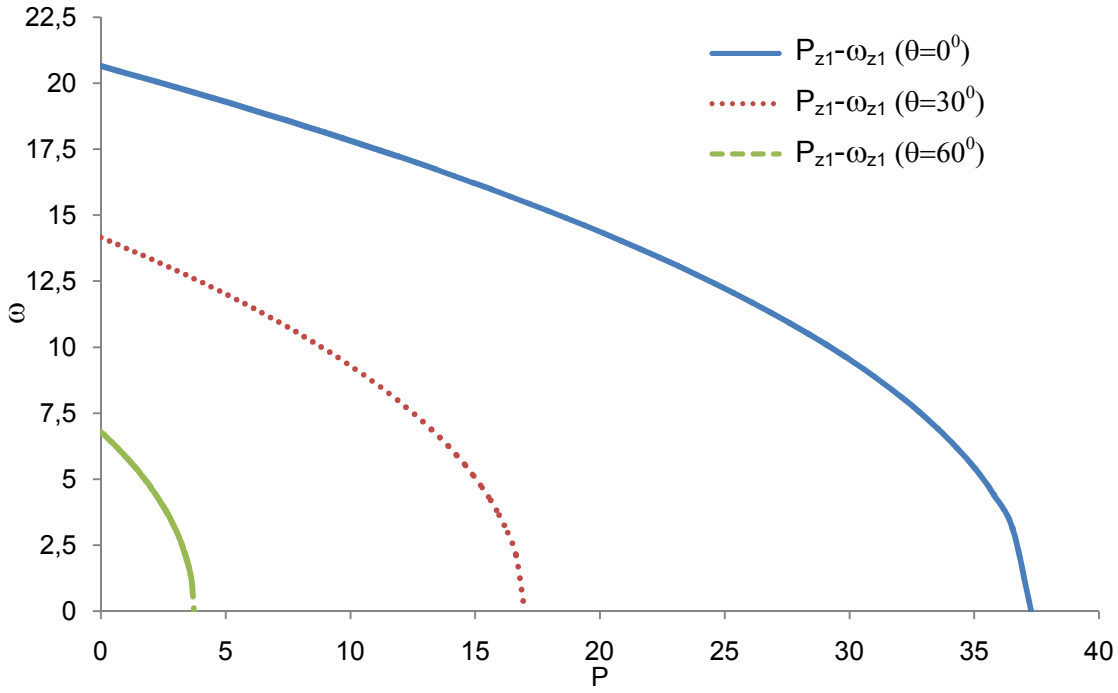

Figure 6: Load-frequency curves of a clamped-clamped anti-symmetric angle-ply $[\theta/-\theta]$ composite beam with the fiber angles 0, 30^0 and 60^0.

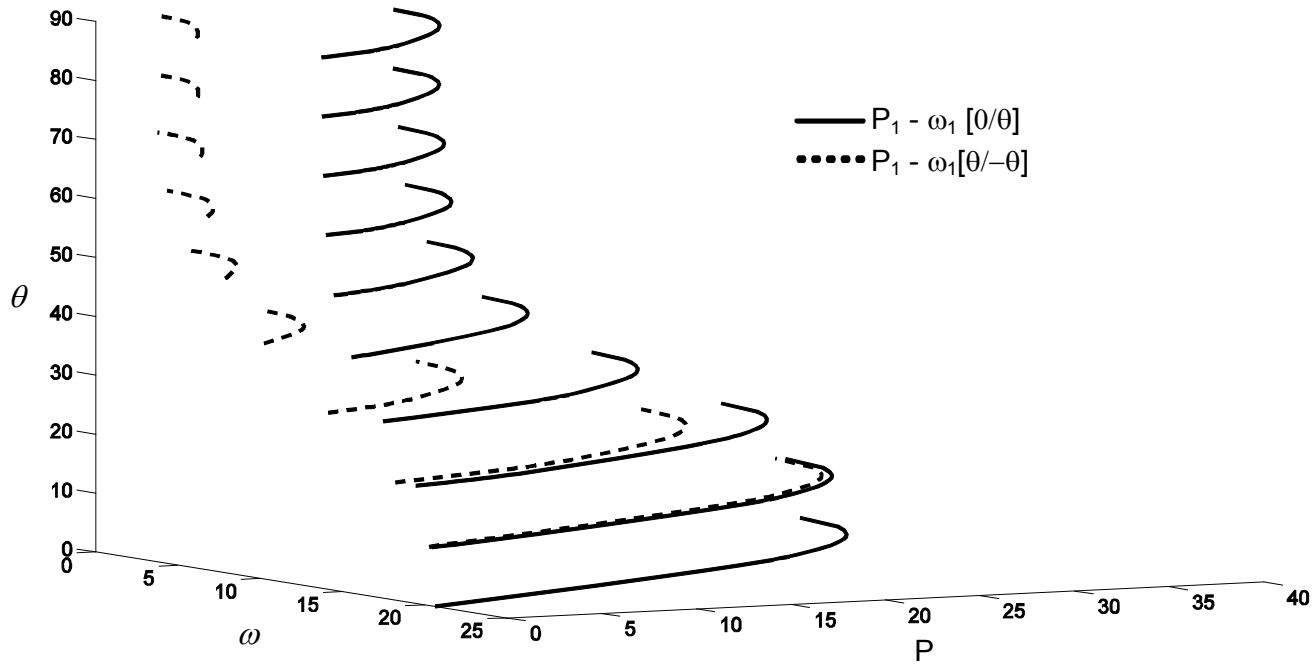

Figure 7: Three dimensional interaction diagram of the fundamental natural frequency, axial force and fiber angle of clamped-clamped composite beams with $[\theta/-\theta]$ and $[0/\theta]$ lay-ups.

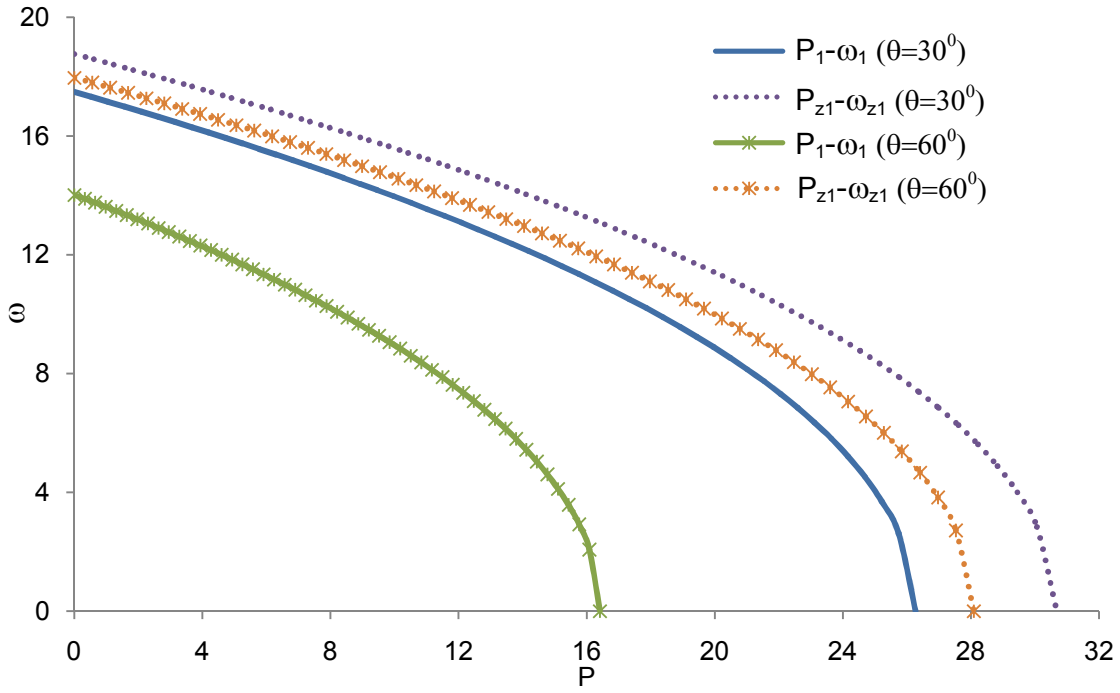

Figure 8: Load-frequency curves of a clamped-clamped unsymmetric $[0/\theta]$ composite beam with the fiber angles 30^0 and 60^0.

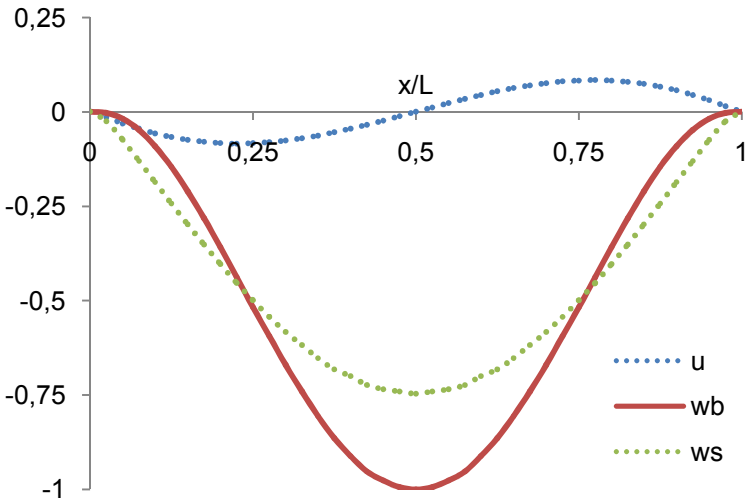

a. First mode shape $\omega_1 = 14.019$.

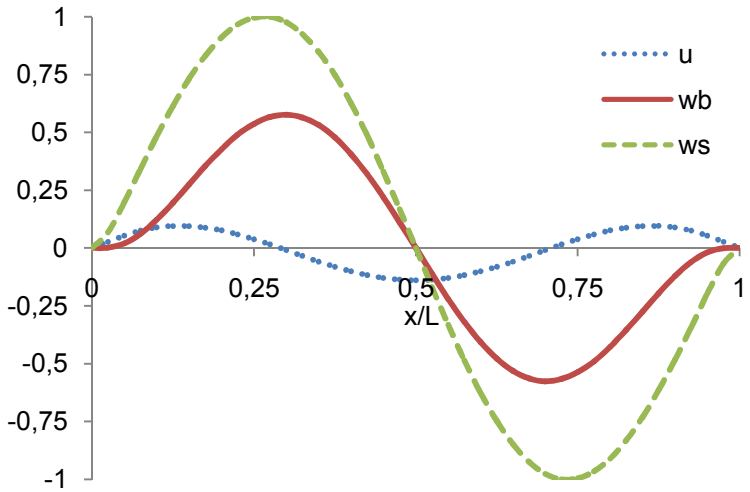

b. Second mode shape $\omega_2 = 34.155$.

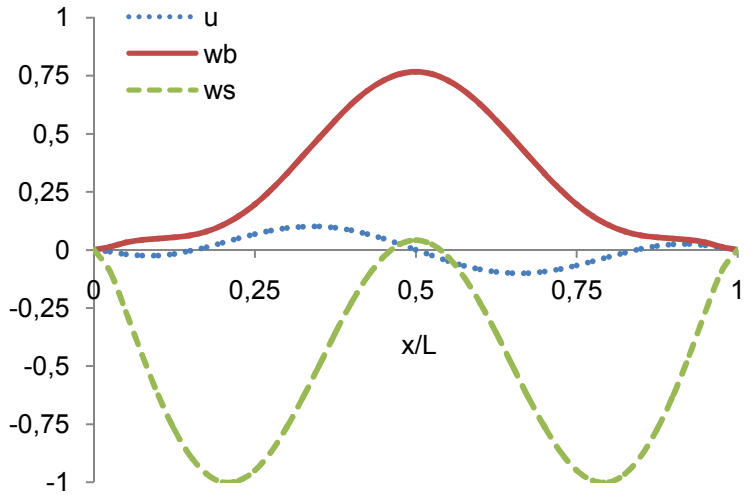

c. Third mode shape $\omega_3 = 57.099$.

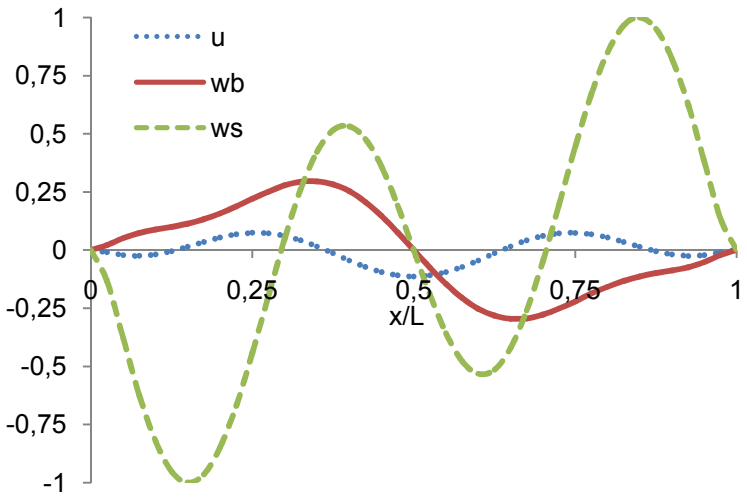

d. Fourth mode shape $\omega_4 = 85.851$

Figure 9: Vibration mode shapes of the axial and flexural components of a clamped-clamped un-symmetric $[0/\theta]$ composite beam with the fiber angle 60^0.

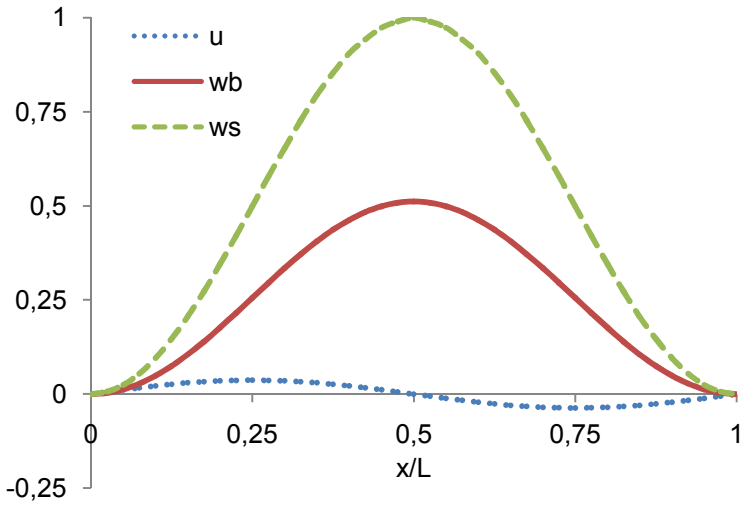

a. P_{cr} = 26.264 with the fiber angle 30^0.

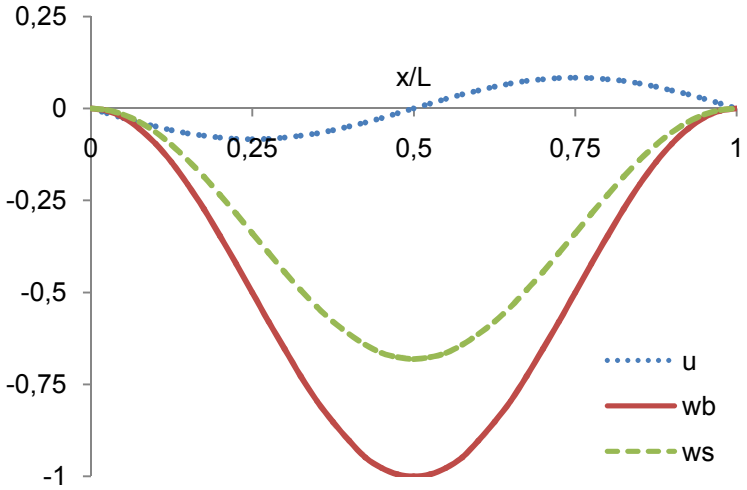

b. P_{cr} = 16.417 with the fiber angle 60^0.

Figure 10: Buckling mode shapes of the axial and flexural components of a clamped-clamped un-symmetric $[0/\theta]$ composite beam with the fiber angles 30^0 and 60^0.

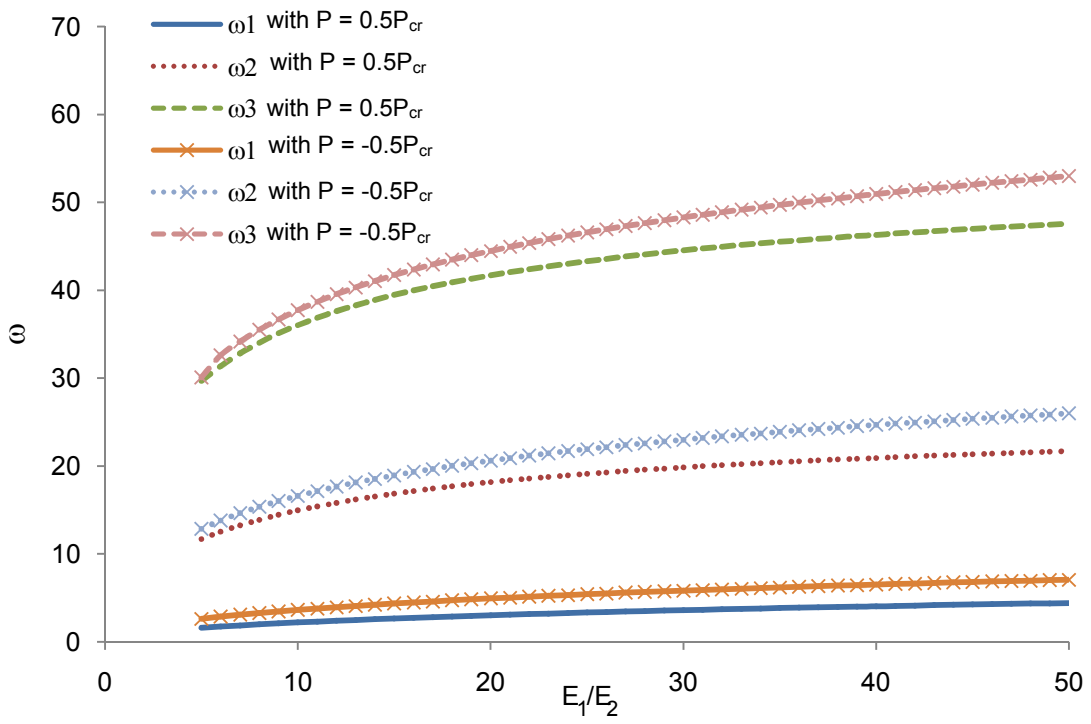

a. Symmetric cross-ply lay-up

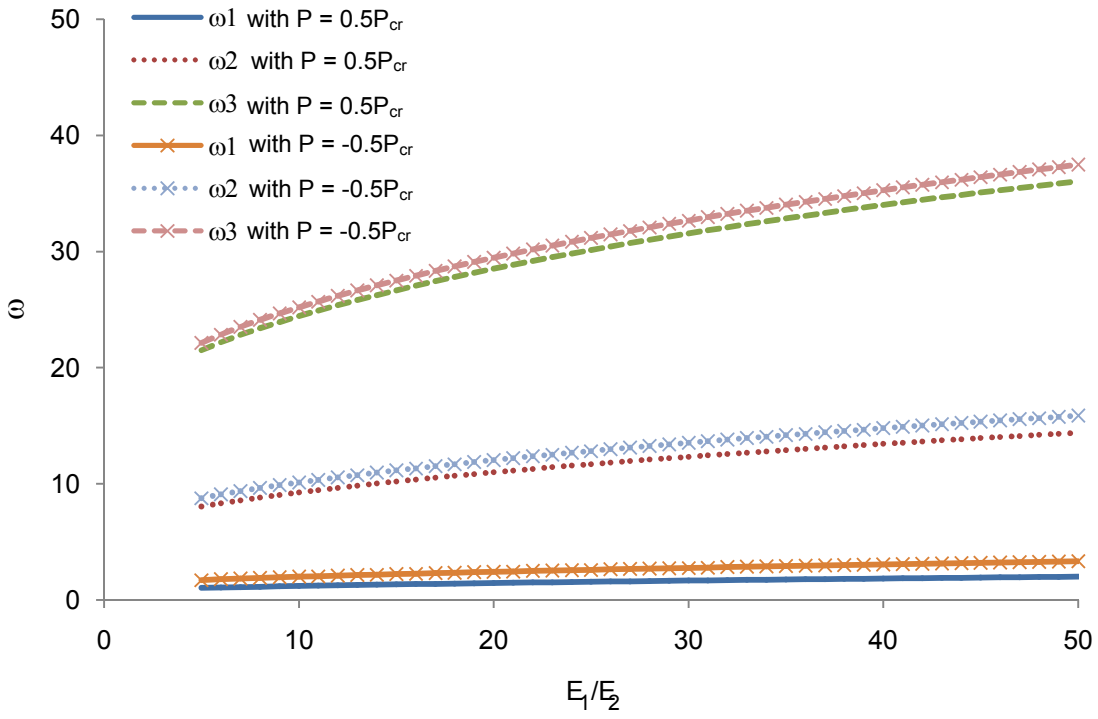

b. Anti-symmetric cross-ply lay-up

Figure 11: Variation of the first three natural frequencies with respect to modulus ratio change of a cantilever composite beam under an axial compressive force $P=0.5P_{cr}$ and tensile force $P=-0.5P_{cr}$